Langmuir

Article

pubs.acs.org/Langmuir

How Chain Plasmons Govern the Optical Response in Strongly Interacting Self-Assembled Metallic Clusters of Nanoparticles

Ruben Esteban,*[,†] Richard W. Taylor,[‡] Jeremy J. Baumberg,[‡] and Javier Aizpurua*[,†]

[†]Material Physics Center CSIC-UPV/EHU and Donostia International Physics Center DIPC, Paseo Manuel de Lardizabal 4 20018, Donostia-San Sebastián Spain

[‡]NanoPhotonics Centre, Cavendish Laboratory, University of Cambridge, CB3 0HE, U.K.

Supporting Information

ABSTRACT: Self-assembled clusters of metallic nanoparticles separated by nanometric gaps generate strong plasmonic modes that support both intense and localized near fields. These find use in many ultrasensitive chemical and biological sensing applications through surface enhanced Raman scattering (SERS). The inability to control at the nanoscale the structure of the clusters on which the optical response crucially depends, has led to the development of general descriptions to model the various morphologies fabricated. Here, we use rigorous electrodynamic calculations to study clusters formed by a hundred nanospheres that are separated by ∼1 nm distance, set by the dimensions of the macrocyclic molecular linker employed experimentally. Three-dimensional (3D) cluster structures of moderate compactness are of special interest since they resemble self-assembled clusters grown under typical diffusion-limited aggregation conditions. We find very good agreement between the simulated and measured far-field extinction spectra, supporting the equivalence of the assumed and experimental morphologies. From these results we argue that the main features of the optical response of two- and three-dimensional clusters can be understood in terms of the excitation of simple units composed of different length resonant chains. Notably, we observe a qualitative difference between short- and long-chain modes in both spectral response and spatial distribution: dimer and short-chain modes are observed in the periphery of the cluster at higher energies, whereas inside the structure longer chain excitation occurs at lower energies. We study in detail different configurations of isolated one-dimensional chains as prototypical building blocks for large clusters, showing that the optical response of the chains is robust to disorder. This study provides an intuitive understanding of the behavior of very complex aggregates and may be generalized to other types of aggregates and systems formed by large numbers of strongly interacting particles.

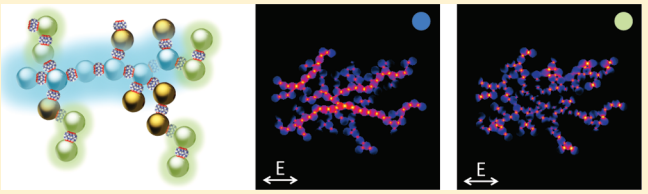

INTRODUCTION

Self-assembly[1,2] offers a favorable route for large-scale, low-cost fabrication of plasmonic structures. The degree of control achievable can be considerably finer than for lithographic or similar top-down fabrication techniques. For clusters of small metallic spheres, it is possible to identify a global topology, parametrized by the fractal dimension, but the position and connectivity of each individual component is random. This lack of nanoscale control does not necessarily obscure reproducible optical properties of the full system, such as the spectral position of the plasmonic resonances or the resulting average values of the Raman enhancement. Understanding and optimizing the optical response of such complex aggregates would be considerably aided by knowledge of the optical response at a local level, where the random nature of the aggregation process influences the response of each individual particle and the system as a whole.

An experimental study of the local response is a highly difficult challenge. Due to the diffraction limit, classical optical microscopy cannot resolve individual (or groups of) particles only tens of nanometers in size. New microscopy techniques may allow better resolution,[3−8] but the systematic optical imaging of complex clusters remains very difficult, especially for three-dimensional structures in solution. From a theoretical perspective, much work has been performed using methods well suited for weakly or moderately interacting clusters, often using simple dipolar models of particle interaction. These provide general trends for very large clusters.[9−12] Most important is the identification of interactions between all particles that cause particularly strong and localized local fields (known as "hot spots"),[13−16] which are critical to explain the electromagnetic contribution to surface enhanced Raman spectroscopy (SERS)[17−20] in clusters, and which can lead to nonlinear effects.[21−23]

Additional physical phenomena are present in strongly interacting particles, a situation that has been widely studied in optical nanoantennas[24−26] formed by a few well-defined constituents. In the simple cases of a dimer formed by two

Special Issue: Colloidal Nanoplasmonics

Received: January 13, 2012
Revised: February 26, 2012
Published: February 26, 2012

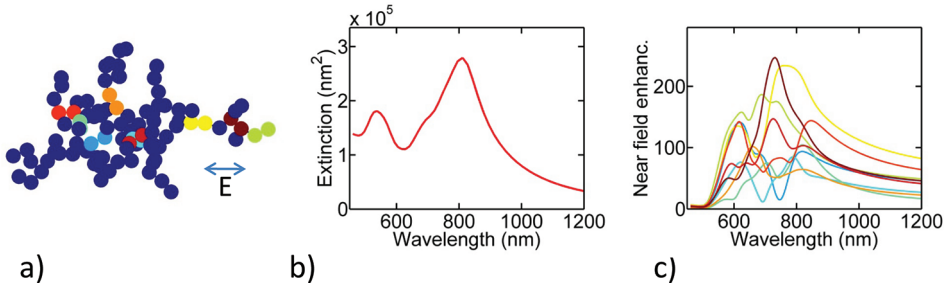

Figure 1. (a) Structure of one of the Au clusters considered, with d = 40 nm and fixed separation distance d_g = 0.9 nm. The structure is three-dimensional, the surrounding medium is water, and the incident plane wave is linearly polarized. (b) Extinction spectra of the geometry in panel a. (c) Spectra of the field enhancement at the center of some of the gaps in panel a. Each spectrum in panel c corresponds to the gap between the two particles of the same color in panel a.

spheres,[27−30] spherical nanoshells,[31,32] or circular disks,[33] the possibility of obtaining strong modal redshifts and intense and strongly confined local fields is found, due to the near-field coupling between the dimer constituents. Here we develop a better understanding of the optical behavior of self-assembled aggregates of many spheres with nanoscale separations.[34] This requires the consideration of both the strong interaction between closely located particles and the presence of a large number of particles forming the complex structures. Previous studies have examined far-field[35,36] and local-field[37] properties in connection[38] with the geometry of the aggregates. We focus here on the behavior of strongly interacting clusters formed by metallic spheres (diameter, d = 10−40 nm) separated by rigid molecular linkers,[39,40] such as cucurbiturils,[1,41] which serve to precisely define the interparticle separation between neighbors at nanoscale distances.[42,43] The reproducibility and precision of the fixed particle separation provides a crucial distinctive feature of the aggregates allowing us to build nanoassemblies with a high degree of control over the optoelectronic response.

As the exact nature of the interparticle gap critically affects the optical resonances of a structure, effective control of the gap distance will result in much increased definition and reproducibility of the local behavior, with different regions of the cluster showing similar field distributions. Along this line of thought, we have suggested in previous work[40,44] that the excitation of plasmonic modes in local one-dimensional chains of different length can be used to explain most of the observed optical behavior from an aggregate, an approach also discussed in works related to branched chain particle networks.[45] However, the decomposition of an aggregate into different one-dimensional chains is not unique, and the modes of each individual chain can be significantly affected by their mutual interaction. Thus, a careful assessment of the simple description of the cluster in terms of its chain modes is required.

Figure 1 introduces the complexity of the local optical behavior that can be found within such self-assembled clusters and that we aim to understand more intuitively in this work. Figure 1a represents a complex three-dimensional cluster of gold spheres with 40 nm diameter and fixed interparticle separation distance of d_g = 0.9 nm. Details of the structures and numerical method are given below. The extinction spectra of this cluster are shown in Figure 1b, with a main resonance peak near λ = 810 nm and a second peak around λ = 540 nm. A small inflection point at $\lambda \sim$ 700 nm suggests the presence of at least one additional resonant mode. Figure 1c shows the corresponding spectra of the near-field enhancement at several gap sites in the same cluster, and demonstrates how complex and variable is the exact site-specific local-field response. The enhancement spectra within the different gap-sites do present some consistencies with peaks that appear at similar frequencies for several of the spectra, but in general the response is strongly dependent on the particular environment of each gap. It does not appear obvious from Figure 1c how to derive general trends about the local optical behavior in particle clusters, in terms of one-dimensional chains or otherwise. In this paper we show how an improved understanding can be obtained.

In the following, we describe the optics of clusters starting from a systematic study of isolated one-dimensional chains with incremental disorder. We argue that considering the optical resonances of the constituent one-dimensional chains of the clusters is indeed useful to reach conclusions about the local and global behavior of the whole structure. From this we then consider full two-dimensional and three-dimensional clusters. We also propose a conceptual difference between the external perimeter of the clusters, where dimers and short chain modes resonant at higher energies are bound, compared to internal regions within the clusters that are dominated by long chain modes at lower energies.

RESULTS

One-Dimensional Chains. It is particularly interesting to study the contribution to the optical response from one-dimensional chains[46−51] that are found embedded within larger two- and three-dimensional aggregates. However, these chains within the aggregate are not straight but kinked and distorted. It is thus important to understand the effect of disorder[52−55] on the optical response.

Considering isolated one-dimensional chains, Figures 2c,e show the extinction spectra for chains formed by a number N = 16 of Au spheres of 40 nm diameter. The structure of the chains ranges from perfectly straight to highly disordered (Figure 2a). All the particles are contained in the plane xy perpendicular to the direction of propagation of the incident plane wave. The disorder is quantified by the circular standard deviation δ. To obtain δ, we first calculate an angle θ_i between a reference direction and the vector $\overline{v}_i$ defined by the axis of each of the $N - 1$ constituent dimers. The sign of $\overline{v}_i$ is always determined by choosing as its origin the particle closer to one fixed end of the chain. The disorder δ is defined as the circular standard deviation of the obtained set of angles, $\delta = (-2 \ln(|1/(N-1)\Sigma_{i=1}^{N-1} e^{i\theta_i}|))^{1/2}$. The use of directional statistics minimizes the problem of ,the modularity of the angle. Neither changing the reference direction used for the definition of θ_i nor choosing the opposite sign for $\overline{v}_i$ affects the obtained δ. Averaged near-field and Raman enhancements are obtained by

dx.doi.org/10.1021/la300198r | Langmuir 2012, 28, 8881−8890

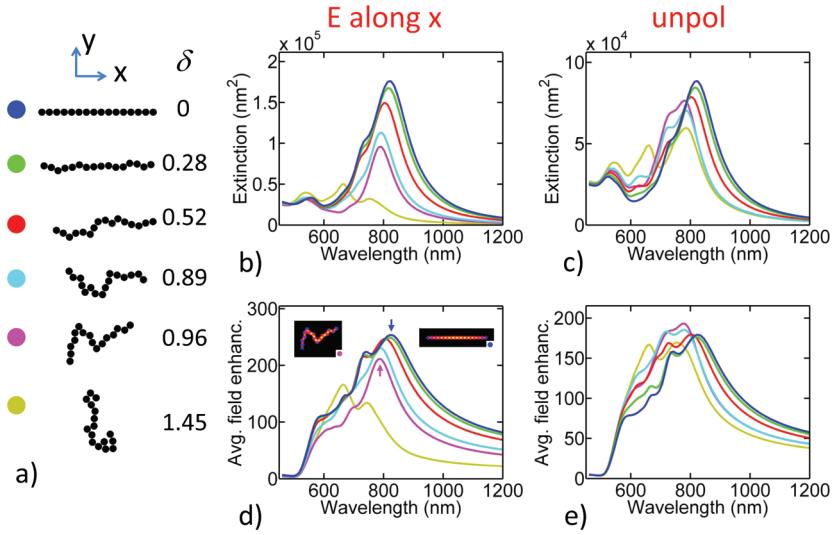

Figure 2. Optical response of isolated one-dimensional chains of 40 nm Au diameter spheres in water with different degrees of disorder δ and with fixed separation gap d_g = 0.9 nm. (a) Schematics of the chains considered, with the associated disorders. The geometry is displayed in the *xy* plane that contains the center of all the spheres and is perpendicular to the direction of propagation of the incoming plane wave. (b,c) Extinction spectra and (d,e) average field enhancement at the gaps for the chains in panel a, considering polarization along the *x* axis (b,d) and unpolarized light (c,e). The color of each line indicate the corresponding geometry according to the indications in panel a. Near-field distributions of two of the modes, marked with arrows, are shown as insets in panel d for two different situations of disorder (δ = 0 and δ = 0.96). The insets represent the electric displacement field in logarithmic color scale.

averaging the field at the gap center for all d_{gap} = 0.9 nm junctions, as detailed in the Methods section.

For a perfectly straight chain[56,57] (δ = 0) with axis parallel to the polarization of the incident plane wave (*x* axis), we observe a peak around λ = 820 nm dominating the spectra for both the extinction (Figure 2b) and the near-field enhancement averaged over all d_{gap} = 0.9 nm gaps (Figure 2d). This peak corresponds to the lowest energy, dipole-like mode. A less pronounced contribution from other higher energy modes appears at $\lambda \sim$ 740 nm, $\lambda \sim$ 670 nm, and $\lambda \sim$ 560 nm. As the incident electric field is perfectly parallel to the chain axis, all these modes are longitudinal. We also plot in Figure 2b,d the evolution of the extinction and average near-field enhancement spectra for chains showing some degree of disorder (see the schematics of the disordered chains in Figure 2a) and under the same conditions of incident field. The weakly disordered chains remain roughly parallel to the incident light polarization. As the disorder increases, the lowest energy peak blueshifts with reduced intensity, while for the largest considered disorder δ = 1.45, a different mode at $\lambda \sim$ 665 nm becomes predominant. Longitudinal modes in the full structure, or in some constituent subchains, explain most of the dominant optical response, but tangential modes can also be excited for $\delta \neq 0$ at frequencies slightly blueshifted with respect to the resonance of the single sphere ($\lambda \sim$ 530 nm). Despite these small differences, the spectra for moderately disordered chains remain remarkably close to the results of the perfectly straight chains, thus suggesting a robust means to simply characterize the optical modes of complex aggregates. As an example, the near-field distribution of two representative modes (λ = 824.7 nm for straight chains, δ = 0, and λ = 786.9 nm for disordered chains, δ = 0.96) are shown as insets in Figure 2d. A relevant near-field enhancement is clearly preserved under disorder.

The response of a chain under linearly polarized light is strongly dependent on the orientation of the chain. To separate this effect from the influence of disorder, it is useful to consider unpolarized illumination. Figure 2c,e shows the extinction and average field enhancement spectra for the same chains as Figure 2b,d but now illuminated with an unpolarized plane wave (see the Methods section for details). For the straight chain, the line shape of the extinction and average enhancement spectra are very similar to that of the polarized light in Figure 2b,d. This is due to the weak interaction of the chain with the polarization perpendicular to its axis (electric field along *y*). The main contribution of this polarization is the excitation of relatively weak transverse modes near $\lambda \sim$ 520 nm. Thus unpolarized light mostly results only in a scaling of the extinction by a factor of 0.5 and of the field enhancement by a factor of $1/\sqrt{2}$, where the latter is due to the assumption of incoherent illumination as explained in the Methods section.

Unpolarized light can excite modes supported in the chains with an efficiency that is independent of the chain orientation in the *xz* plane, or the orientation of particular subchains forming the complete structure. As disorder can affect the chain orientation, δ affects the lowest order mode of the structures in Figure 2a less strongly for unpolarized light than for *x*-polarized light. This weaker dependence with δ can be observed both in the extinction (Figure 2b,c) and in the near-field enhancement (Figure 2d,e). Notably, the extinction maximum associated with this mode diminishes by less than ~35%, and the corresponding near-field enhancement remains almost unchanged or even slightly larger for $\delta \neq 0$ compared to the straight chains (δ = 0). Unpolarized light can also excite more efficiently the higher order modes, as revealed by examining the peaks at lower wavelengths, notably for δ = 0.89.

Figure 3 examines in more detail the effect of disorder on the lowest energy peak from chains formed by a different number *N* of *d* = 40 nm gold particles. The smaller chains (N < 16) are subchains of the largest ones (N = 16), and the exact geometry for N = 16 and δ = 0, 0.28, 0.52, 0.89, 0.96, and 1.45 correspond to the structures shown in Figure 2a. In general, the random nature of the process introduces a statistical scattering of the results as δ is increased, but general trends can be outlined as marked by solid lines in Figure 3. Nevertheless, the

dx.doi.org/10.1021/la300198r | Langmuir 2012, 28, 8881−8890

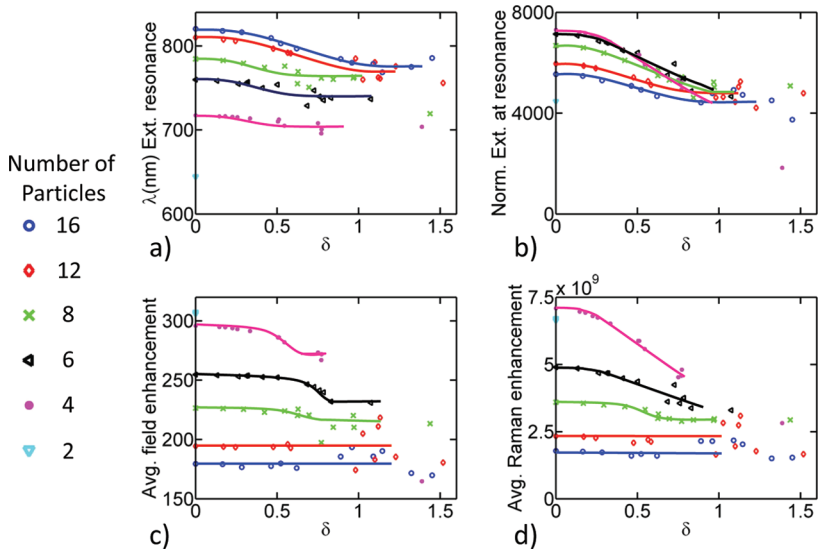

Figure 3. Effect of disorder on the lowest energy mode of one-dimensional chains in water formed by 40 nm diameter Au spheres with fixed separation gap d_g = 0.9 nm. (a) Wavelength of lowest energy extinction maximum. (b) Extinction value normalized to the number of particles. Each point in panel b corresponds to the wavelengths obtained in panel a. (c) Field enhancement and (d) Raman signal enhancement averaged over the different gaps at the corresponding lowest energy extinction maximum. In all graphs, the calculated results for chains of different number of particles are given by the symbols indicated at the left. The solid lines are plotted as guides to the eye.

exact trends as a function of δ may depend on the particular conditions of growth. We are interested in the general robustness of the optical response to disorder, and not in the particular quantitative results.

Figure 3(a) show the spectral position of the lowest energy extinction peak for different disorders and chain lengths. In general, a larger N redshifts the resonance[54,56,57] while increasing the disorder acts to blueshift it. This blueshift, which is small or moderate ($\lesssim$7% of the δ = 0 value), is less marked in the shorter chains. As a consequence, the difference between the peak position characterizing the long and short chains becomes smaller for increasing disorder δ. In some cases of relatively large disorder, a particular chain can show a resonance at a slightly lower wavelength than a shorter chain of similar δ. This inversion can be attributed to the random nature of the structures. Figure 3b shows the extinction values at the resonant wavelengths obtained in Figure 3a, normalized by the number of particles in the chain. The extinction is strongest for the perfectly straight chains, and presents a clear but mild tendency to lose strength as the disorder increases. The weakening of the extinction is more pronounced for short chains and less significant for longer ones.

Next we show the effect of disorder on the field enhancement (Figure 3c) and on the Raman signal enhancement for a characteristic Raman mode of the cucurbituril linking molecule at 826 cm^{-1}(Figure 3d),[58] both averaged over all gaps that the cucurbituril defines experimentally. The field and Raman enhancement is calculated for each chain at the wavelength corresponding to the respective lowest energy resonance peak. This resonant wavelength depends on N and δ similarly to the values displayed in Figure 3a for the extinction peak. Increasing the disorder of short chains tends to diminish the average field and Raman enhancement obtained. The reduction is however quite moderate,[59] which is a highly relevant result for these structures considering previous work demonstrating a typically large sensitivity of Raman measurements in plasmonic systems to relatively small geometrical changes[60] (for fixed gap systems). Furthermore, for large chains, there is no clear trend as disorder δ increases, and the influence of the disorder remains small. In some cases, the presence of disorder can even result in slightly larger enhancements. It is reasonable to assume that this stronger enhancement has a similar origin as the hot spots found on rough surfaces or in aggregates of weakly interacting particles. The demonstrated robustness of the Raman enhancement to the presence of disorder is highly relevant to explain the strength of the experimentally measured Raman scattering in similar complex self-assembled aggregates. This stability of the optical response in one-dimensional chains under different levels of disorder is preserved for a fixed aspect ratio of the full chain (length of the chain/radius) given mainly by the number of particles forming the chain. Similar stabilities in optical response have been identified both theoretically and experimentally in similar systems showing long-range interactions[52,53,55] and even in metamaterials.[61,62] Our results thus point toward a similar effect, with the number of particles being the key aspect in producing the stability of the response (assuming a fixed gap distance as in our case), independent of the disorder of the whole chain.

Two-Dimensional Aggregates. Next we present two-dimensional Au clusters,[34,63,64] in which all the particle aggregation occurs within the same plane, as given in Figure 4c–f. Illumination is from a linearly polarized plane wave propagating perpendicularly to the plane containing the spheres. The diameter of the spheres is 40 nm. A dendritic-like morphology of the aggregates has been adopted in the simulations with the cluster generated from a particle seed. It is therefore possible to observe chain-like subunits in the resulting structures, consistent with the expectation for aggregates in diffusion-limited reactions.[40] The extinction cross-section in Figure 4a shows several different resonances, with a dominant peak at λ~755 nm, a weaker maximum at $\lambda \sim$ 545 nm, and two shoulders at $\lambda \sim$ 680 nm and $\lambda \sim$ 865 nm. The latter corresponds to the lowest energy mode of the structures. The field enhancement in Figure 4b also reveals the presence of a similar spectral distribution of modes. Here we show the

dx.doi.org/10.1021/la300198r | Langmuir 2012, 28, 8881–8890

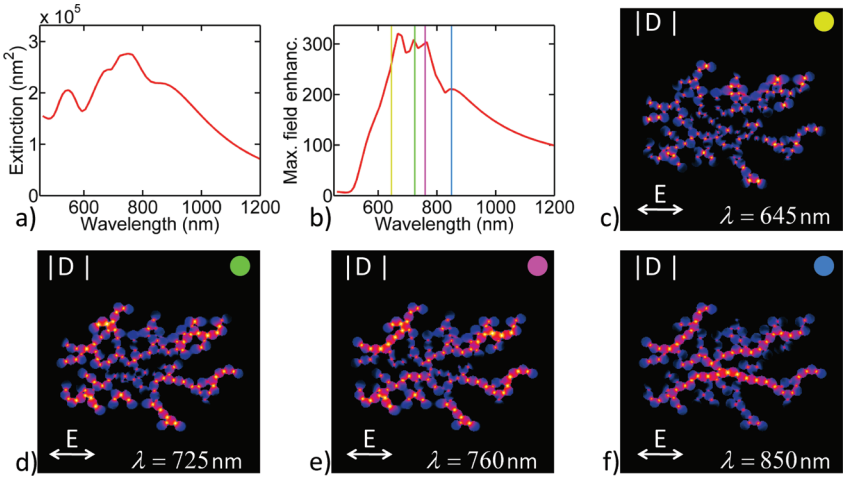

Figure 4. Optical properties of a two-dimensional cluster of 100 Au spheres in water with 40 nm diameter and fixed separation gap d_g = 0.9 nm, illuminated by a linearly polarized plane wave. Spectra for (a) extinction and (b) maximum field enhancement at the gaps. (c–f) Spatial distribution of the electric displacement field in the plane containing the center of the spheres, for λ = (c) 645 nm, (d) 725 nm, (e) 760 nm, and (f) 850 nm, corresponding to the vertical lines in panel b. The values in panels c–f are normalized to the incident planewave amplitude and are expressed in logarithmic scale. In all the graphs, the propagation direction is perpendicular to the plane containing the particles. The polarization is indicated in all the field maps. The area of all the maps is 900 × 900 nm^2.

spectrum of the maximum field enhancement at the gap centers, rather than the average over the different gaps to better emphasize the presence of different modes. The averaged field enhancement reaches values of up to ∼120. A direct correspondence between the spectral position of the peaks and shoulders observed in the extinction and the peaks found in the maximum field enhancement spectrum cannot be established. The latter appear at $\lambda \sim$ 680 nm, $\lambda \sim$ 725 nm, $\lambda \sim$ 760 nm, and $\lambda \sim$ 850 nm. This difference is expected[65,66] given the different nature of the field enhancement (which is determined locally at each position) and the far field (an integrated result of the full structure)

To obtain a better understanding of the excited modes, it is convenient to examine the local behavior of the fields at the aggregate by mapping the spatial field distribution. Figures 4c–f show the electric displacement in the plane through the middle of the spheres, for wavelengths corresponding to the enhancement maxima in Figure 4b and at the frequency λ = 645 nm corresponding to the resonance of an isolated dimer. We plot the electric displacement D to visualize the distribution more clearly. A striking evolution of the excited modes appears for the different wavelengths. For the shortest wavelengths, different dimer or short chains at the periphery of the aggregate exhibit particularly strong displacement fields. As the energy decreases, long chains that can extend toward the center of the structure begin to dominate. The orientation of these chains tends to be roughly parallel to that of the polarization.

The excitation at larger wavelengths in Figure 4 corresponds to the longest of the chains. The more efficient excitation of chains extending roughly parallel to the incident field is consistent with the results for the isolated one-dimensional chains. The aggregate cannot be separated into independent chains, but it is nonetheless possible to distinguish the local excitation of short and long chain modes at wavelengths close to those obtained for the one-dimensional example, and with a similar dependence on polarization.

We discuss in the following why such local modes are present, and the reason for the preference of the short chain modes to be localized at the exterior of the aggregate. If we consider a dimer oriented roughly parallel to the electric field, and linked to the rest of the aggregate by a chain extending in the perpendicular direction, one can expect significantly stronger interaction between the two particles forming the dimer than between the dimer and the rest of the aggregate. Under these conditions, the dimer should behave as if it were isolated, with the corresponding resonance at relatively high energy. An analogous isolation effect can also appear for other short chains longer than the dimer. Critically, the excitation of such short dimer-like chain modes at large energy depends on weak-coupling to the rest of the aggregate, a condition which would be more easily found at the periphery, where each dimer is surrounded by fewer particles. We thus believe that the possibility of weaker interaction between a dimer and the rest of the structure at the exterior of an aggregate explains why the high-energy dimer-like chain modes often appear in this region. By contrast, longer chains requiring the interaction between many particles forming a chain do not depend on such structural isolation and may also be less influenced by interaction with other chains. As a result, such longer chains are found all over the aggregate.

The results of Figure 4 support the assertion that one can interpret the optics of two-dimensional clusters in terms of the excitation of different local chains of different lengths. This is most apparent from the clearly distinguished spatial field distributions in Figure 4c–f, but the extinction and near-field spectra of Figure 4a,b can also be understood as the result of different contributions from one-dimensional chains of the type studied in Figures 2 and 3. We find that the lowest energy peak of the two-dimensional aggregate extinction and enhancement both appear near λ = 855 nm ($\lambda \sim$ 885 for the scattering), and thus is moderately redshifted ($\Delta\lambda \sim$ 50 nm) with respect to the resonance of the largest isolated one-dimensional chain considered (Figure 3). We argue that this shift is caused by interaction between different chains within the aggregate, an interaction that is more important in this two-dimensional geometry. With the particles confined to two dimensions, the incident plane wave considered illuminates all of the particles with the same phase, allowing for a particularly significant

dx.doi.org/10.1021/la300198r | Langmuir 2012, 28, 8881–8890

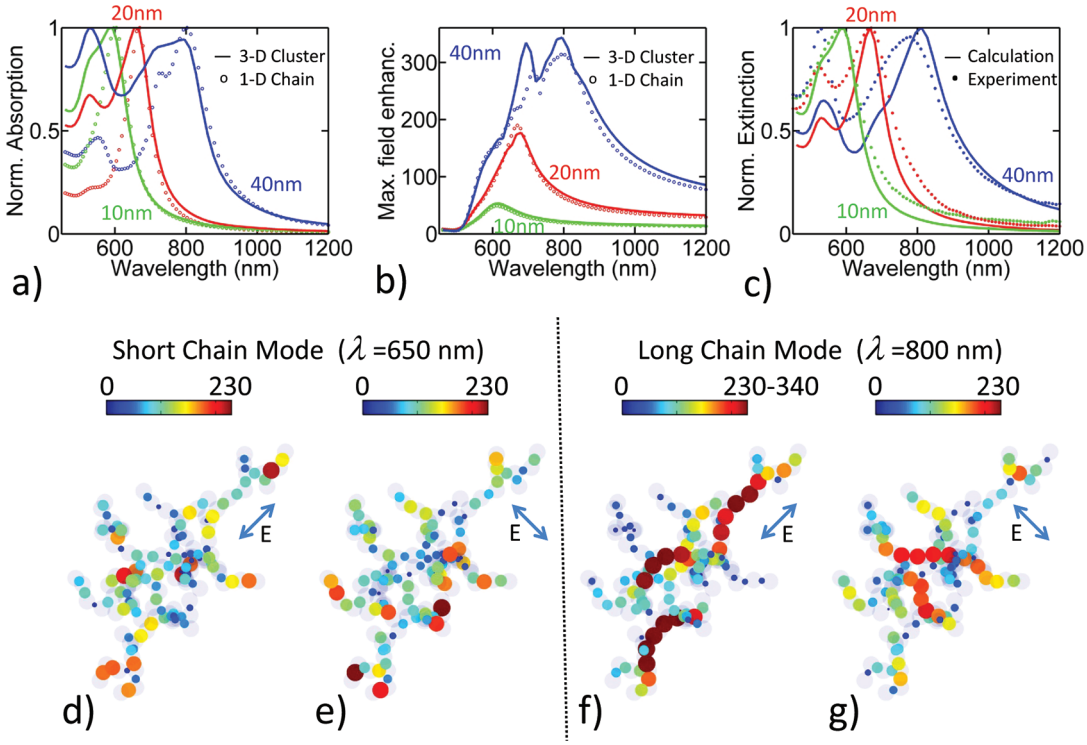

Figure 5. Optical properties of a three-dimensional Au cluster in water, with fixed separation gap d_g = 0.9 nm and different diameters (d = 10, 20, and 40 nm) of the 100 constituent spheres. The aggregate for d = 40 nm is displayed in panels d–g and also in Figure 1a. For other diameters, the positions of the spheres corresponding to d = 40 nm are simply multiplied by a constant factor to maintain the 0.9 nm gap distance, and the general morphology of the aggregate is thus unchanged. Calculated (a) absorption normalized to the maximum value and (b) maximum of the field enhancement at the gaps, under linearly polarized light, for the three-dimensional clusters (solid line) and for a chain of 16 spheres with moderate disorder of δ = 0.52 (open circles; see Figure 2a for the one-dimensional morphology). (c) Extinction normalized to the maximum value for the three-dimensional cluster calculation (solid line) and from experimental aggregates (solid circles), for unpolarized light. The numbers indicated in panels a–c correspond to the diameter of the spheres. (d–g) Values of the field enhancement at the gaps for different wavelengths and two orthogonal polarizations. The wavelengths are (d,e) λ = 650 nm and (f,g) λ = 800 nm. The polarization is indicated in the plots. The semitransparent blue spheres correspond to the d = 40 nm spheres forming the aggregate, and the solid color spheres denote the strength of the fields at the center of the gaps, both by their color and their size, i.e., the area of these spheres is proportional to the field strength. We plot the projection of the cluster into a plane perpendicular to the propagation direction. The polarization and propagation direction in panels a and b for the simulated clusters correspond to the direction marked in panels d and f, and for the chain the electric field is along the x axis indicated in Figure 2a. Unpolarized light with the same propagation direction is considered in panel c for comparison with the experiments.

constructive modal superposition. To support this, we simulated the two-dimensional cluster with oblique incidence. In this instance (not shown), the phase of the illumination changes in the plane containing the particles, and the lowest energy peak position blueshifts ($\Delta\lambda \sim 40$ nm) and recovers a position much closer to the resonance of the long isolated one-dimensional chain, in agreement with our expectation. Coherent scattering from many chains can also lead to radiative broadening[65,67] and possibly explains the relatively slow decay of the extinction signal in Figure 4a for large wavelengths. The decay is significantly faster for oblique illumination, probably also due to the smaller influence of the constructive superposition discussed above.

Three-Dimensional Aggregates. We next consider the properties of three-dimensional clusters, which are especially relevant in many experimental situations produced by chemical synthesis. The three-dimensional structure is also generated from a particle seed, with an intermediate compactness, consistent with the experimental growth observed. We first relate the optics of these aggregates with the results of one-dimensional chains considered in isolation. Figure 5a,b shows the absorption spectra and maximum near-field enhancement for such a three-dimensional cluster and for a moderately disordered (δ = 0.52) one-dimensional chain of 16 Au particles, with particle diameters d = 10 nm, d = 20 nm, or d = 40 nm and under linearly polarized plane wave illumination. The axis of the chain is roughly parallel to the polarization. Figure 5d–g and Figure 1a show the morphology of the cluster, and Figure 2a shows that of the chain, for d = 40 nm. For other diameters, the position of the spheres is scaled by a factor that preserves the gap width, d_{gap} = 0.9 nm. We consider the absorption instead of the extinction cross-section because the influence of the scattering on the spectral shape can be more significant in the three-dimensional cluster than in the one-dimensional chains.

As expected, the dominant optical behavior of the clusters can be captured by the properties of single one-dimensional chains, as demonstrated by the maximum field enhancement at the center of the gaps (Figure 5b) and the absorption spectra (Figure 5a). In addition to the very good agreement for the spectral position and long wavelength decay of the lowest order mode for all diameters considered, the simple chain also reproduces some of the features of the clear higher-order aggregate resonant contribution present for particles of d = 40 nm near $\lambda \sim 710$ nm. We have also found in related work[44] that the wavelength position of the lowest energy extinction peak

dx.doi.org/10.1021/la300198r | Langmuir 2012, 28, 8881–8890

behaves similarly when comparing one-dimensional chains of increasing length to randomly grown three-dimensional aggregates of the particle sizes considered here. The lowest energy mode in Figure 5a is, however, more predominant in the spectra of the one-dimensional chain than for the three-dimensional aggregates, which is consistent with many different modes contributing to the optical response of the latter.

The striking similarities between the absorption and enhancement spectra of one- and three-dimensional structures offer further support to the critical importance of local linear chains to explain the optical response of the cluster. To further examine the excitation of these local chain modes, we consider the spatial distribution of the fields in a similar fashion to the case of the two-dimensional chains. Figure 5d−g shows the field enhancement at the center of the gaps of the three-dimensional clusters under study. We consider d = 40 nm and two perpendicular polarizations to demonstrate how the orientation of the incident field determines which chain modes are excited efficiently. Two wavelengths are considered, one (λ = 800 nm) corresponding to the lowest energy mode and another (λ = 650 nm) close to the resonance of an isolated dimer. The maps obtained show a complex modal structure, which could be expected in random three-dimensional structures. Nonetheless, the general trends are clearly consistent with the results found in the two-dimensional aggregate: dimers located on the fringe generally provide the largest field enhancement for the higher-energy excitation, while lower-energy excitation results in strong fields within gaps distributed along chains of several particles. The resonant chains are approximately parallel to the incident field, as made evident when switching the polarization: (Figure 5d versus Figure 5e and also Figure 5f versus Figure 5g).

Comparison with Experimental Results. Figure 5c shows the extinction spectra for the three-dimensional clusters shown in Figure 5d−g, together with experimental measurements for aggregates of spheres of the same nominal size and gap separation distance. The agreement is good for the three d = 10 nm, d = 20 nm, and d = 40 nm diameters considered, particularly after appreciating that the exact morphology of the experimental clusters is not known. The position of the lowest energy peak is very well predicted by the calculations, as well as the presence of a second peak near the resonant wavelength of the single sphere, where tangential modes and higher order longitudinal modes can contribute to the spectra. The relative weight of both peaks is not the same for experiments and theory, but the discrepancies found are not surprising, as the modeling does not consider the exact experimental configuration.

The spectra of the lowest energy mode for d = 40 nm decays at large wavelengths very similarly in the experiments and in the calculations. The description of this long-wavelength tail by an equation normally used to describe dipolar resonances of simple systems is explained in detail elsewhere.[44] The agreement becomes somewhat worse for smaller particles, which we attribute to the scattering contribution to the extinction. For all considered sizes, the absorption dominates the extinction in the case of a single isolated sphere. However, assuming a very simple model with constructive interference from all particles and no interaction, the absorption cross-section of a cluster scales with the number of particles N and the scattering with N^2. Thus, the relative contribution of the latter to the extinction becomes more important for large clusters. This strong additional contribution leads to radiative damping, which broadens the peaks. However, the broadening from radiative damping and the $\sim N^2$ scaling of the scattering is based on the assumption that the scattering from all particles adds up constructively, which is not the case for sufficiently large three-dimensional clusters. Thus, the significance of these effects should only increase up to a certain physical size of the aggregate, where the critical parameter is the dimensions of the cluster in nanometers compared to the incident wavelength, and not the number of particles. We suggest that the cluster modeled here is sufficiently large for d = 40 nm to capture most of the radiative broadening present in the larger experimental clusters, but is not large enough to reproduce all the broadening for the case of d = 20 nm and d = 10 nm. An alternative explanation might be that the experimental clusters are constituted by a smaller number of particles for larger d.

CONCLUSIONS AND DISCUSSION

This paper discusses ways to easily interpret the response of complex experimental clusters formed by strongly interacting plasmonic nanospheres. These aggregates show intermediate compactness (fractal dimension), typical for diffusion-limited growth,[68] and it is possible to visually distinguish local one-dimensional chains formed by several adjacent particles separated by the fixed gap distance d_{gap}. We are able to interpret the observed optical behavior of a large aggregate whose structure is unknown by identifying the optical response to be composed of contributions from smaller functional one-dimensional chains embedded within.

As self-assembled clusters are likely to not contain perfectly straight chains, we first systematically analyzed the effect of disorder δ on the optical properties of one-dimensional chains. The chain extinction is robustly preserved under increasing disorder, especially under unpolarized illumination, with significant deviations mainly due to the excitation of higher order modes for certain δ values. Notably, the broad lowest energy mode that dominates much of the response is only weakly affected by the presence of disorder. This study thus strongly supports the presence of clear resonant chain modes even when the position and connectivity of strongly interacting particles is not controlled. The observed robustness of the results to disorder should hold when the one-dimensional chains are embedded in either two- or three-dimensional clusters.

The far-field and the maximum enhancement spectra of two- and three-dimensional clusters are generally consistent with the interpretation of the optical response in terms of local one-dimensional chain modes. These spectra correspond to the global response of the complete cluster. The spatial distribution of the local fields for two- and three-dimensional aggregates clearly support the presence and key role of these chain modes. At high frequencies, notably near the dipolar resonance of an isolated dimer, strong fields tend to be confined to dimers (or short chains) at the periphery of the structures. This behavior is consistent with the resonant excitation at the end of a chain of a few particles that are oriented approximately perpendicularly to the rest of the chain. As the wavelength increases, the field enhancement can be significant along longer chains that can extend toward the center of the structure, with resonant frequencies generally compatible with the modes supported by isolated one-dimensional long chains. The incident polarization selects which particular chain modes are more efficiently excited.

dx.doi.org/10.1021/la300198r | Langmuir 2012, 28, 8881−8890

The interpretation of the optics of clusters in terms of individual chains brings up the question of to what extent coupling between different chains is important. We have discussed, for instance, how coherent scattering from different chains can lead to a larger scattering contribution to the extinction. We are more especially interested here in the position and spectral width of the lowest energy mode, as it is difficult to separate contributions from other modes. Both a redshift and a broadening with respect to the isolated chains were clearly observed for the lowest energy mode in two-dimensional clusters, which we attributed mainly to the interaction between chains for the case of constant phase of the excitation field at the position of all spheres. By contrast, for three-dimensional clusters, no clear effect of the interaction on the spectral position of the modes was apparent in the absorption and extinction, and the broadening of the lowest energy mode was more modest. Thus, for the geometries considered here, we do not need to invoke coupling between chains to explain the main observations in the optics of three-dimensional clusters, which are of special interest in experiments. Interaction though may be stronger for larger spheres and more compact aggregates, even though the description of the optics of two- and three-dimensional clusters in terms of the excitation of chain modes is very robust for the intermediate compactness studied in this work.

The current study assumed a fixed gap distance and identical particles, a relevant situation for experimental work of aggregates with rigid molecular linkers. It is nonetheless an interesting question to what extent the conclusions would hold if these parameters vary across the structures. As the resonance depends critically on the ratio between the separation distance and the particle's size, variations in this ratio will result in larger differences between different regions of the cluster, with resonant contributions expanding into a broader inhomogenous spectrum. If the size ratios vary strongly within the clusters, it may be difficult to find modes extending along very long chains. The description of the optical response of the aggregate in terms of different chains may nonetheless remain valid: dimers at the periphery of the clusters dominating the high-energy response, and chain modes being more significant for the long-wavelength region of the spectra.

In conclusion, our work found local one-dimensional chains of different length to be the critical element explaining the resonances of self-assembled clusters, thus offering a simple interpretation of the very complex structures grown experimentally. Notably, we have observed a spectral and spatial distinction between resonant modes extending along short and long chains within the cluster. Short chains resonate at a larger energy and are typically found at the periphery, while longer chains are excited at a lower energy and extend all over the aggregate. The results obtained should be particularly useful to interpret measurements that depend on the local behavior, such as Raman spectroscopy of molecules located at the cluster gaps.[18,19,40,69,70] The validity of the results for relevant experimental conditions is supported by the good agreement between the calculated and measured spectra in aggregates formed by particles of different sizes.

METHODS

Calculations. The calculations consider clusters and chains of gold particles of different diameters d under plane wave illumination. The distance between a particle and its closest neighbor is 0.9 nm, and all clusters are placed in water, modeled as an infinite space with dielectric constant $\varepsilon = 1.77$. The gold dielectric constant is taken from Johnson and Christy,[71] size corrected according to refs 12 and 72 by $\varepsilon(\omega) = \varepsilon_{JC} - \omega_p{}^2/(\omega(\omega + i\gamma_c)) + \omega_p^2/(\omega(\omega + i\gamma_p))$. ω is the frequency, ε_{JC} is the experimentally measured bulk value, and $\omega_p = 9.065$ eV and $\gamma_p = 0.0708$ eV are the plasma frequency and damping frequency, respectively, of a drude model describing the bulk values. $\gamma_c = \gamma_p + v_f/R$ encodes the size correction, with v_F being the Fermi velocity and R the radius of the particles $R = d/2$.

To obtain the cluster and chain morphology for the theoretical study, we start from an initial single particle seed. The structures are generated by the random and progressive addition of new spherical particles at a 0.9 nm distance from the closest neighbor. The 0.9 nm distance is chosen to reflect the interparticle spacing determined by the cucurbituril linker, which is assumed not to affect the optical properties, i.e., no area of different dielectric constant than water is present in the gap. After imposing some general conditions (dimensionality, level of disorder, etc.), the exact position of each particle is determined with a pseudo-random number generator to mimic the lack of control in the experimental positions. We define "contiguous spheres" as those separated by exactly 0.9 nm, and the axis of a dimer is the vector joining the center of two contiguous spheres. In two- and three-dimensional clusters, the chains are defined as sets of several contiguous particles within the clusters that extend in a roughly linear direction with an axis along a mean chain orientation, defined with respect to the first and last particle of the chain.

We obtain the far-field properties (absorption, scattering, and extinction cross-section) and the near-field behavior as a function of incident wavelength λ. In particular, we analyze the field enhancement at the center of each 0.9 nm gap, defined as the field amplitude E normalized by the value for the incident radiation E_0. $|E/E_0|^2$ is the local intensity enhancement, and the Stokes Raman enhancement is simply obtained by the standard ratio $|E(\omega_{in})/E_0|^2|E(\omega_{out})/E_0|^2$, with ω_{in} and ω_{out} being the incident and emitted frequencies, respectively, for a Raman shift of 826 cm^{-1}. In the Raman expression, $|E(\omega_{in})/E_0|^2$ corresponds to the excitation of the molecule, and $|E(\omega_{out})/E_0|^2$ is assumed to describe the emission process, which is often a good approximation due to reciprocity considerations.[73] As the shift between ω_{in} and ω_{out} is small compared with the broadness of typical plasmonic resonances, the Raman signal approximately scales with the fourth power of the field enhancement. We calculate the enhancement at the center of the gaps, and obtain the average enhancement over all 0.9 nm gaps of the cluster, as well as the maximum enhancement. For the latter, the gap with the strongest field at each frequency is selected. For averaging between different gaps, a simple arithmetic mean value is used. When obtaining the enhancement in each of the gaps for unpolarized illumination, we assume two incoherent orthogonal polarizations and average over the local intensity I. We take the square root of this value to obtain the field enhancement, and the square of the averaged value of $(I(\omega_{in})I(\omega_{out}))^{1/2}$ to obtain the Raman enhancement.[74] These choices ensure that rotating an aggregate or chain in the plane perpendicular to the propagation direction of the incident field does not affect the averaged enhancement. From the definition, if one of the polarization components does not interact with the chains, the obtained field enhancement is $1/\sqrt{2}$ times the value for the other component.

To numerically solve the classical electrodynamic equations, we use the multiple multipole (MMP) method, OpenMaX.[75] For the separation distances considered here within the linear regime, quantum effects should be negligible.[76−78] The MMP method allows one to describe the fields by mathematical expansions, such as multipoles and Bessel expansions, which are solutions of the homogeneous Maxwell equations. For the clusters of spherical particles considered in this paper, the main difference between MMP and the standard T-Matrix method[79] is that the former also offers the possibility to expand the fields at positions different than the center of the particles at the aggregate. In particular, we use extra multipoles centered near the narrow gaps to better describe the interaction between closely located spheres. A numerical routine finds the coefficients of the expansions that minimize the error in the functions of the fields set by the boundary conditions. The

convergence of the results looks excellent for the one-dimensional chains, and highly satisfactory for the two- and three-dimensional clusters (see the Supporting Information for details).

Experimental Methods. Curcurbit[5]uril was synthesized using methods reported elsewhere.[1] A 1.2 mMol solution was prepared and used to induce coagulation in 1 mL of a citrate-capped gold nanoparticle solution (manufactured by BBI, used as supplied). The concentration of cucurbit[5]uril ensured that the aggregation kinetics were in the diffusion-limited regime. Extinction spectroscopy was performed in real time during the aggregation phase.

■ ASSOCIATED CONTENT

Supporting Information

Study of convergence of the results. This material is available free of charge via the Internet at http://pubs.acs.org/.

■ AUTHOR INFORMATION

Corresponding Author

*E-mail: ruben_esteban@ehu.es (R.E.); aizpurua@ehu.es (J.A.).

Notes

The authors declare no competing financial interest.

■ ACKNOWLEDGMENTS

We acknowledge funding from EPSRC EP/F059396/1, EP/G060649/1 and EU NanoSci-E+ CUBiHOLE grants, and project ETORTEK2011 from the Department of Industry of the Basque Government, and FIS2010-19609-C02-C01 and EUI200803816 from the Spanish Ministry of Science and Technology.

■ REFERENCES

(1) Lee, T.-C.; Scherman, O. A. Formation of dynamic aggregates in water by cucurbit[5]uril capped with gold nanoparticles. *Chem. Commun.* **2010**, *46*, 2438−2440.

(2) Grzelczak, M.; Vermant, J.; Furst, E. M.; Liz-Marzán, L. M. Directed self-assembly of nanoparticles. *ACS Nano* **2010**, *4*, 3591−3605.

(3) Nelayah, J.; Kociak, M.; Stephan, O.; García de Abajo, F. J.; Tence, M.; Henrard, L.; Taverna, D.; Pastoriza-Santos, I.; Liz-Marzán, L. M.; Colliex, C. Mapping surface plasmons on a single metallic nanoparticle. *Nat. Phys.* **2007**, *3*, 348−353.

(4) Esteban, R.; Vogelgesang, R.; Dorfmüller, J.; Dmitriev, A.; Rockstuhl, C.; Etrich, C.; Kern, K. Direct near-field optical imaging of higher order plasmonic resonances. *Nano Lett.* **2008**, *8*, 3155−3159.

(5) Hell, S. W. Microscopy and its focal switch. *Nat. Methods* **2009**, *6*, 24−32.

(6) Schnell, M.; García-Etxarri, A.; Huber, A. J.; Crozier, K.; Aizpurua, J.; Hillenbrand, R. Controlling the near-field oscillations of loaded plasmonic nanoantennas. *Nat. Photonics* **2009**, *3*, 287−291.

(7) Vogelgesang, R.; Dmitriev, A. Real-space imaging of nanoplasmonic resonances. *Analyst* **2010**, *135*, 1175−1181.

(8) Cang, H.; Labno, A.; Lu, C.; Yin, X.; Liu, M.; Gladden, C.; Liu, Y.; Zhang, X. Probing the electromagnetic field of a 15-nanometre hotspot by single molecule imaging. *Nature* **2011**, *469*, 385−388.

(9) Liebsch, A.; Persson, B. N. J. Optical properties of small metallic particles in a continuous dielectric medium. *J. Phys. C: Solid State Phys.* **1983**, *16*, 5375.

(10) Persson, B. N. J.; Liebsch, A. Optical properties of two-dimensional systems of randomly distributed particles. *Phys. Rev. B* **1983**, *28*, 4247−4254.

(11) Markel, V. A.; Shalaev, V. M.; Stechel, E. B.; Kim, W.; Armstrong, R. L. Small-particle composites. I. Linear optical properties. *Phys. Rev. B* **1996**, *53*, 2425−2436.

(12) Kreibig, U.; Vollmer, M. *Optical Properties of Metal Clusters*; Springer: New York, 1995.

(13) Stockman, M. I.; Pandey, L. N.; Muratov, L. S.; George, T. F. Giant fluctuations of local optical fields in fractal clusters. *Phys. Rev. Lett.* **1994**, *72*, 2486−2489.

(14) Shalaev, V. M.; Botet, R.; Tsai, D.; Kovacs, J.; Moskovits, M. Fractals: Localization of dipole excitations and giant optical polarizabilities. *Physica A* **1994**, *207*, 197−207.

(15) Stockman, M. I. Inhomogeneous eigenmode localization, chaos, and correlations in large disordered clusters. *Phys. Rev. E* **1997**, *56*, 6494−6507.

(16) Safonov, V. P.; Shalaev, V. M.; Markel, V. A.; Danilova, Y. E.; Lepeshkin, N. N.; Kim, W.; Rautian, S. G.; Armstrong, R. L. Spectral dependence of selective photomodification in fractal aggregates of colloidal particles. *Phys. Rev. Lett.* **1998**, *80*, 1102−1105.

(17) Moskovits, M. Surface-enhanced spectroscopy. *Rev. Mod. Phys.* **1985**, *57*, 783−826.

(18) Kneipp, K.; Wang, Y.; Kneipp, H.; Perelman, L. T.; Itzkan, I.; Dasari, R. R.; Feld, M. S. Single molecule detection using surface-enhanced Raman scattering (SERS). *Phys. Rev. Lett.* **1997**, *78*, 1667−1670.

(19) Nie, S.; Emory, S. R. Probing single molecules and single nanoparticles by surface-enhanced Raman scattering. *Science* **1997**, *275*, 1102−1106.

(20) Haynes, C. L.; Van Duyne, R. P. Plasmon-sampled surface-enhanced Raman excitation spectroscopy. *J. Phys. Chem. B* **2003**, *107*, 7426−7433.

(21) Shalaev, V. M.; Poliakov, E. Y.; Markel, V. A. Small-particle composites. II. Nonlinear optical properties. *Phys. Rev. B* **1996**, *53*, 2437−2449.

(22) Danckwerts, M.; Novotny, L. Optical frequency mixing at coupled gold nanoparticles. *Phys. Rev. Lett.* **2007**, *98*, 026104.

(23) Kim, S.; Jin, J.; Kim, Y.-J.; Park, I.-Y.; Kim, Y.; Kim, S.-W. High-harmonic generation by resonant plasmon field enhancement. *Nature* **2008**, *453*, 757−760.

(24) Balanis, C. A. *Antenna Theory: Analysis and Design*; Wiley-Interscience: Hoboken, NJ, 2005.

(25) Muhlschlegel, P.; Eisler, H.-J.; Martin, O. J. F.; Hecht, B.; Pohl, D. W. Resonant optical antennas. *Science* **2005**, *308*, 1607−1609.

(26) Novotny, L. Effective wavelength scaling for optical antennas. *Phys. Rev. Lett.* **2007**, *98*, 266802.

(27) Xu, H.; Aizpurua, J.; Käll, M.; Apell, P. Electromagnetic contributions to single-molecule sensitivity in surface-enhanced Raman scattering. *Phys. Rev. E* **2000**, *62*, 4318−4324.

(28) Rechberger, W.; Hohenau, A.; Leitner, A.; Krenn, J. R.; Lamprecht, B.; Aussenegg, F. R. Optical properties of two interacting gold nanoparticles. *Opt. Commun.* **2003**, *220*, 137−141.

(29) Nordlander, P.; Oubre, C.; Prodan, E.; Li, K.; Stockman, M. I. Plasmon hybridization in nanoparticle dimers. *Nano Lett.* **2004**, *4*, 899−903.

(30) Romero, I.; Aizpurua, J.; Bryant, G. W.; Abajo, F. J. G. D. Plasmons in nearly touching metallic nanoparticles: singular response in the limit of touching dimers. *Opt. Express* **2006**, *14*, 9988−9999.

(31) Lassiter, J. B.; Aizpurua, J.; Hernandez, L. I.; Brandl, D. W.; Romero, I.; Lal, S.; Hafner, J. H.; Nordlander, P.; Halas, N. J. Close encounters between two nanoshells. *Nano Lett.* **2008**, *8*, 1212−1218.

(32) Pérez-González, O.; Zabala, N.; Borisov, A. G.; Halas, N. J.; Nordlander, P.; Aizpurua, J. Optical spectroscopy of conductive junctions in plasmonic cavities. *Nano Lett.* **2010**, *10*, 3090−3095.

(33) Gunnarsson, L.; Rindzevicius, T.; Prikulis, J.; Kasemo, B.; Käll, M.; Zou, S.; Schatz, G. C. Confined plasmons in nanofabricated single silver particle pairs: Experimental observations of strong interparticle interactions. *J. Phys. Chem. B* **2005**, *109*, 1079−1087.

(34) Girard, C.; Dujardin, E.; Li, M.; Mann, S. Theoretical near-field optical properties of branched plasmonic nanoparticle networks. *Phys. Rev. Lett.* **2006**, *97*, 100801.

(35) Lindsay, H. M.; Lin, M. Y.; Weitz, D. A.; Sheng, P.; Chen, Z.; Klein, R.; Meakin, P. Properties of fractal colloid aggregates. *Faraday Discuss. Chem. Soc.* **1987**, *83*, 153−165.

(36) Lattuada, M.; Ehrl, L. Scattering properties of dense clusters of colloidal nanoparticles. *J. Phys. Chem. B* **2009**, *113*, 5938−5950.

(37) Quinten, M. Local fields close to the surface of nanoparticles and aggregates of nanoparticles. *Appl. Phys. B: Lasers Opt.* **2001**, *73*, 245−255.
(38) Karpov, S.; Gerasimov, V.; Isaev, I.; Podavalova, O.; Slabko, V. The origin of anomalous enhancement of electromagnetic fields in fractal aggregates of metal nanoparticles. *Colloid J.* **2007**, *69*, 159−169.
(39) Lim, D.-K.; Jeon, K.-S.; Hwang, J.-H.; Kim, H.; Kwon, S.; Suh, Y. D.; Nam, J.-M. Highly uniform and reproducible surface-enhanced Raman scattering from DNA-tailorable nanoparticles with 1-nm interior gap. *Nat. Nanotechnol.* **2011**, *6*, 452−460.
(40) Taylor, R. W.; Lee, T.-C.; Scherman, O. A.; Esteban, R.; Aizpurua, J.; Huang, F. M.; Baumberg, J. J.; Mahajan, S. Precise subnanometer plasmonic junctions for SERS within gold nanoparticle assemblies using cucurbit[*n*]uril "glue". *ACS Nano* **2011**, *5*, 3878−3887.
(41) Lagona, J.; Mukhopadhyay, P.; Chakrabarti, S.; Isaacs, L. The cucurbit[*n*]uril family. *Angew. Chem., Int. Ed.* **2005**, *44*, 4844−4870.
(42) Ward, D. R.; Grady, N. K.; Levin, C. S.; Halas, N. J.; Wu, Y.; Nordlander, P.; Natelson, D. Electromigrated nanoscale gaps for surface-enhanced Raman spectroscopy. *Nano Lett.* **2007**, *7*, 1396−1400.
(43) Ward, D. R.; Hüser, F.; Pauly, F.; Cuevas, J. C.; Natelson, D. Optical rectification and field enhancement in a plasmonic nanogap. *Nat. Nanotechnol.* **2010**, *5*, 732−736.
(44) Taylor, R. W. et al. To be published.
(45) Lin, S.; Li, M.; Dujardin, E.; Girard, C.; Mann, S. One-dimensional plasmon coupling by facile self-assembly of gold nanoparticles into branched chain networks. *Adv. Mater.* **2005**, *17*, 2553−2559.
(46) Markel, V. Coupled-dipole approach to scattering of light from a one-dimensional periodic dipole structure. *J. Mod. Opt.* **1993**, *40*, 2281−2291.
(47) Krenn, J. R.; Dereux, A.; Weeber, J. C.; Bourillot, E.; Lacroute, Y.; Goudonnet, J. P.; Schider, G.; Gotschy, W.; Leitner, A.; Aussenegg, F. R.; Girard, C. Squeezing the optical near-field zone by plasmon coupling of metallic nanoparticles. *Phys. Rev. Lett.* **1999**, *82*, 2590−2593.
(48) Maier, S. A.; Brongersma, M. L.; Kik, P. G.; Atwater, H. A. Observation of near-field coupling in metal nanoparticle chains using far-field polarization spectroscopy. *Phys. Rev. B* **2002**, *65*, 193408.
(49) Weber, W. H.; Ford, G. W. Propagation of optical excitations by dipolar interactions in metal nanoparticle chains. *Phys. Rev. B* **2004**, *70*, 125429.
(50) Alù, A.; Engheta, N. Theory of linear chains of metamaterial/plasmonic particles as subdiffraction optical nanotransmission lines. *Phys. Rev. B* **2006**, *74*, 205436.
(51) Koenderink, A. F.; Polman, A. Complex response and polariton-like dispersion splitting in periodic metal nanoparticle chains. *Phys. Rev. B* **2006**, *74*, 033402.
(52) Markel, V. A.; Sarychev, A. K. Propagation of surface plasmons in ordered and disordered chains of metal nanospheres. *Phys. Rev. B* **2007**, *75*, 085426.
(53) Alu, A.; Engheta, N. Effect of small random disorders and imperfections on the performance of arrays of plasmonic nanoparticles. *New J. Phys.* **2010**, *12*, 013015.
(54) Barrow, S. J.; Funston, A. M.; Gómez, D. E.; Davis, T. J.; Mulvaney, P. Surface plasmon resonances in strongly coupled gold nanosphere chains from monomer to hexamer. *Nano Lett.* **2011**, *11*, 4180−4187.
(55) Rüting, F. Plasmons in disordered nanoparticle chains: Localization and transport. *Phys. Rev. B* **2011**, *83*, 115447.
(56) Citrin, D. S. Plasmon polaritons in finite-length metal-nanoparticle chains: The role of chain length unravelled. *Nano Lett.* **2005**, *5*, 985−989.
(57) Arnold, M. D.; Blaber, M. G.; Ford, M. J.; Harris, N. Universal scaling of local plasmons in chains of metal spheres. *Opt. Express* **2010**, *18*, 7528−7542.
(58) Mahajan, S.; Lee, T.-C.; Biedermann, F.; Hugall, J. T.; Baumberg, J. J.; Scherman, O. A. Raman and SERS spectroscopy of cucurbit[*n*]urils. *Phys. Chem. Chem. Phys.* **2010**, *12*, 10429−10433.
(59) Ghenuche, P.; Cormack, I. G.; Badenes, G.; Loza-Alvarez, P.; Quidant, R. Cavity resonances in finite plasmonic chains. *Appl. Phys. Lett.* **2007**, *90*, 041109.
(60) Schuck, P. J.; Fromm, D. P.; Sundaramurthy, A.; Kino, G. S.; Moerner, W. E. Improving the mismatch between light and nanoscale objects with gold bowtie nanoantennas. *Phys. Rev. Lett.* **2005**, *94*, 017402.
(61) Rockstuhl, C.; Lederer, F.; Etrich, C.; Zentgraf, T.; Kuhl, J.; Giessen, H. On the reinterpretation of resonances in split-ring-resonators at normal incidence. *Opt. Express* **2006**, *14*, 8827−8836.
(62) Boudarham, G.; Feth, N.; Myroshnychenko, V.; Linden, S.; García de Abajo, J.; Wegener, M.; Kociak, M. Spectral imaging of individual split-ring resonators. *Phys. Rev. Lett.* **2010**, *105*, 255501.
(63) Girard, C.; Dujardin, E.; Baffou, G.; Quidant, R. Shaping and manipulation of light fields with bottom-up plasmonic structures. *New J. Phys.* **2008**, *10*, 105016.
(64) Su, H.; Li, Y.; Li, X.-Y.; Wong, K. S. Optical and electrical properties of Au nanoparticles in two-dimensional networks: An effective cluster model. *Opt. Express* **2009**, *17*, 22223−22234.
(65) Le, F.; Brandl, D. W.; Urzhumov, Y. A.; Wang, H.; Kundu, J.; Halas, N. J.; Aizpurua, J.; Nordlander, P. Metallic nanoparticle arrays: A Common substrate for both surface-enhanced Raman scattering and surface-enhanced infrared absorption. *ACS Nano* **2008**, *2*, 707−718.
(66) Chen, J.; Albella, P.; Pirzadeh, Z.; Alonso-González, P.; Huth, F.; Bonetti, S.; Bonanni, V.; Åkerman, J.; Nogués, J.; Vavassori, P.; Dmitriev, A.; Aizpurua, J.; Hillenbrand, R. Plasmonic nickel nanoantennas. *Small* **2011**, *7*, 2341−2347.
(67) Willingham, B.; Link, S. Energy transport in metal nanoparticle chains via sub-radiant plasmon modes. *Opt. Express* **2011**, *19*, 6450−6461.
(68) Lin, M. Y.; Lindsay, H. M.; Weitz, D. A.; Klein, R.; Ball, R. C.; Meakin, P. Universal diffusion-limited colloid aggregation. *J. Phys.: Condens. Matter* **1990**, *2*, 3093.
(69) Xu, H.; Bjerneld, E. J.; Käll, M.; Börjesson, L. Spectroscopy of single hemoglobin molecules by surface enhanced Raman scattering. *Phys. Rev. Lett.* **1999**, *83*, 4357−4360.
(70) Dadosh, T.; Sperling, J.; Bryant, G. W.; Breslow, R.; Shegai, T.; Dyshel, M.; Haran, G.; Bar-Joseph, I. Plasmonic control of the shape of the Raman spectrum of a single molecule in a silver nanoparticle dimer. *ACS Nano* **2009**, *3*, 1988−1994.
(71) Johnson, P. B.; Christy, R. W. Optical constants of the noble metals. *Phys. Rev. B* **1972**, *6*, 4370−4379.
(72) Berciaud, S.; Cognet, L.; Tamarat, P.; Lounis, B. Observation of intrinsic size effects in the optical response of individual gold nanoparticles. *Nano Lett.* **2005**, *5*, 515−518.
(73) Esteban, R.; Laroche, M.; Greffet, J.-J. Influence of metallic nanoparticles on upconversion processes. *J. Appl. Phys.* **2009**, *105*, 033107−033107−10.
(74) The averaged Raman enhancement is weighted by a factor of 3/2. With this choice, the Raman enhancement obtained for an aggregate that responds only to one of the directions of polarization of the incident light is reduced by a factor 3/8. This factor comes from the evaluation of the integral $1/(2\pi)\int_0^{2\pi} \cos^4(\alpha)\, d\alpha$.
(75) Sannomiya, T.; Vörös, J.; Hafner, C. Symmetry decomposed multiple multipole program calculation of plasmonic particles on substrate for biosensing applications. *J. Comput. Theor. Nanosci.* **2009**, *6*, 749−756.
(76) Mao, L.; Li, Z.; Wu, B.; Xu, H. Effects of quantum tunneling in metal nanogap on surface-enhanced Raman scattering. *Appl. Phys. Lett.* **2009**, *94*, 243102.
(77) Zuloaga, J.; Prodan, E.; Nordlander, P. Quantum description of the plasmon resonances of a nanoparticle dimer. *Nano Lett.* **2009**, *9*, 887−891.
(78) Esteban, R. et al. To be published.
(79) Mackowski, D. W. Calculation of total cross sections of multiple-sphere clusters. *J. Opt. Soc. Am. A* **1994**, *11*, 2851−2861.